Available online at www.sciencedirect.com
SCIENCE DIRECT®
International Journal of Heat and Mass Transfer 49 (2006) 2020–2032
International Journal of HEAT and MASS TRANSFER
www.elsevier.com/locate/ijhmt

Improvement in device performance on laminar counterflow concentric circular heat exchangers with uniform wall fluxes

Chii-Dong Ho *, Shih-Cheng Yeh

Department of Chemical and Materials Engineering, Tamkang University, Tamsui, Taipei 251, Taiwan, ROC

Received 12 October 2005; received in revised form 9 January 2006
Available online 6 March 2006

Abstract

The effects of recycle at the ends on the heat transfer through a concentric circular tube with uniform wall fluxes are studied analytically by an orthogonal expansion technique with eigenfunction power series expansion. The heat transfer problem is solved for fully developed laminar velocity profiles in a double-pass circular heat exchanger with ignoring axial conduction and fluid properties of temperature independence. Analytical results show the external recycle can enhance the heat transfer efficiency compared with that in an open tube (without an impermeable circular tube inserted and without recycle). The compensation between the forced-convection increment and heat-transfer driving force decrement are used to study the heat transfer behavior. The effects of the impermeable-tube location on heat transfer efficiency enhancement as well as the power consumption increment have been also discussed.

Keywords: Conjugated Graetz problem; Concentric circular tubes; Double-pass operation; Heat transfer; Uniform wall fluxes

1. Introduction

Under the assumption of the negligible axial conduction or diffusion, the problem of heat or mass transfer at steady state is known as the classical Graetz problem [1,2]. The conjugated Graetz problem refers to the original problem coupling through mutual conditions with two or more contiguous phases or streams by conjugating the governing equations in each phase (or each stream) [3–9]. The conjugated Graetz problems have been successfully reduced to Sturm–Liouville systems and studied analytically, and would be indeed of practical and theoretical importance.

Some authors have reported that the recycle effect were investigated numerically [10,11] and theoretically [12–14] and has large influences on heat and mass exchangers which in turn play an important role in the device performance. According to the results of the device with recycle, increasing the fluid velocity due to the external recycle in double-pass heat and mass exchangers enhances the transfer coefficient of the desired effect. In contrast, the recyclic operation also produces an undesired effect of preheating (or premixing) by reducing the temperature (or concentration) driving force. Previous literatures suggested that the desirable effect of increasing the convective transfer coefficient suppresses the undesirable effect of decreasing the transfer driving force in double-pass operations, resulting in improved device performance. In fact, many separation processes and reactor designs in chemical engineering were widely used in absorption, fermentation and polymerization for countercurrent operations with internal or external recycle at the ends of the device, such as such as loop reactors [15,16], air-lift reactors [17,18] and draft-tube bubble columns [19,20].

Recently, we have investigated theoretically the recycle effects on the heat or mass transfer rate to the problem with prescribed wall temperature or concentration (Dirichlet problem). The present study is an extension of the work

* Corresponding author. Tel.: +886 2 2621 5656; fax: +886 2 2620 9887.
E-mail address: cdho@mail.tku.edu.tw (C.-D. Ho).

0017-9310/$ - see front matter © 2006 Elsevier Ltd. All rights reserved.
doi:10.1016/j.ijheatmasstransfer.2006.01.004

Nomenclature

a_1	constant defined by Eq. (20)
a_2, a_3	integration constants in Eqs. (22) and (24)
b_1	constant defined by Eq. (21)
b_2, b_3	integration constants in Eqs. (23) and (25)
c_1	constant defined by Eq. (66)
C_p	heat capacity, J/kg k
D	hydraulic mean diameter, m
d_{mn}	coefficient in the eigenfunction $F_{a,m}$
e_{mn}	coefficient in the eigenfunction $F_{b,m}$
F_m	eigenfunction associated with eigenvalue λ_m
g_c	conversion factor kg m/s^2 N
Gz	Graetz number, $4V/\alpha\pi L$
G_m	function defined during the use of orthogonal expansion method
$\bar{h}$	average heat transfer coefficient, kW/m^2 K
h_f	friction loss in conduit, m^2/s^2
H	functions defined by Eqs. (20) and (21)
I_h	heat transfer improvement, defined by Eq. (78)
I_p	power consumption increment, defined by Eqs. (80) and (81)
k	thermal conductivity of the fluid, kW/m K
L	conduit length, m
M	recycle ratio, reverse volume flow rate divided by input volume flow rate
$\overline{Nu}$	Nusselt number
P	hydraulic dissipated energy, hp
Pr	Prandtl number
q''	heat flux, defined by Eqs. (7), (61), (70) and (73), W/m^2
R	inside radius of the outer tube, m
r	radial coordinate, m
Re	Reynolds number
S	expansion coefficient associated with eigenvalue λ_m
T	temperature of fluid, K
V	input volume flow rate of conduit, m^3/s
v	velocity distribution of fluid, m/s
W_1, W_2	constants defined in Eq. (7)
z	axial coordinate, m

Greek symbols

α	thermal diffusivity of fluid, m^2/s
δ	thickness of impermeable sheet, m
η	transversal coordinate, r/R
θ	defined by Eq. (12)
κ	channel thickness ratio
λ_m	eigenvalue
μ	fluid viscosity, kg/m s
ξ	longitudinal coordinate, $\xi = z/(L\,Gz)$
ρ	fluid density, kg/m^3
ϕ	define in Eq. (12)
ψ	dimensionless temperature, $k(T - T_i)/q''R$
$\bar{\psi}$	dimensionless bulk temperature of ψ

Subscripts

a	inner channel
b	annulus channel
F	at the outlet of a double-pass device
i	at the inlet
L	at the end of conduit, $\xi = 1/Gz$
0	in a single-pass device without recycle
w	at the wall surface

of Ho et al. [21] to include the case of the Neumann boundary condition for the conjugated Graetz problem of which the heat flux at the tube wall has been specified. It is believed that the availability of such a solution methodology as developed here for concentric circular tubes with more general boundary conditions is the value in the present work and will be a straightforward manner design and analyze multistream or multiphase problems with recycle coupling mutual conditions at the boundaries.

The purposes of the present study are: (a) to provide the solution to the conjugated Graetz problems for the system in which the uniform energy fluxes at the walls are specified; (b) to study theoretically the recycle effect on the transfer efficiency enhancement in a double-pass heat exchanger. Therefore, the analytical solution obtained is as simple in form and the procedure unquestionably occurs in dealing with many further possible boundary conditions to the corresponding conjugated Graetz problem.

2. Mathematical formalisms

An impermeable sheet with negligible thickness δ ($\ll 2R$) and thermal resistance is inserted in parallel as the inner tube with diameter of $2\kappa R$, which is to divide a open circular tube with length L and inside diameter $2R$ into two parts, inner and annular channels, as shown in Fig. 1(a) and (b) for flow patterns A and B, respectively. Under this design condition, before entering the inner tube for a double-pass operations (flow pattern A), as shown in Fig. 1(a), the fluid with volumetric flow rate V and the inlet temperature T_i will mix with the fluid of volumetric flow rate MV exiting from the annular channel. Counter-current flow is achieved with the aid of conventional pump situated at the end of the inner channel and the flow rate then may be regulated. The inlet fluid may flow through the annular channel with premixing the external recycle exiting from the inner channel (flow pattern B), as shown in Fig. 1(b).

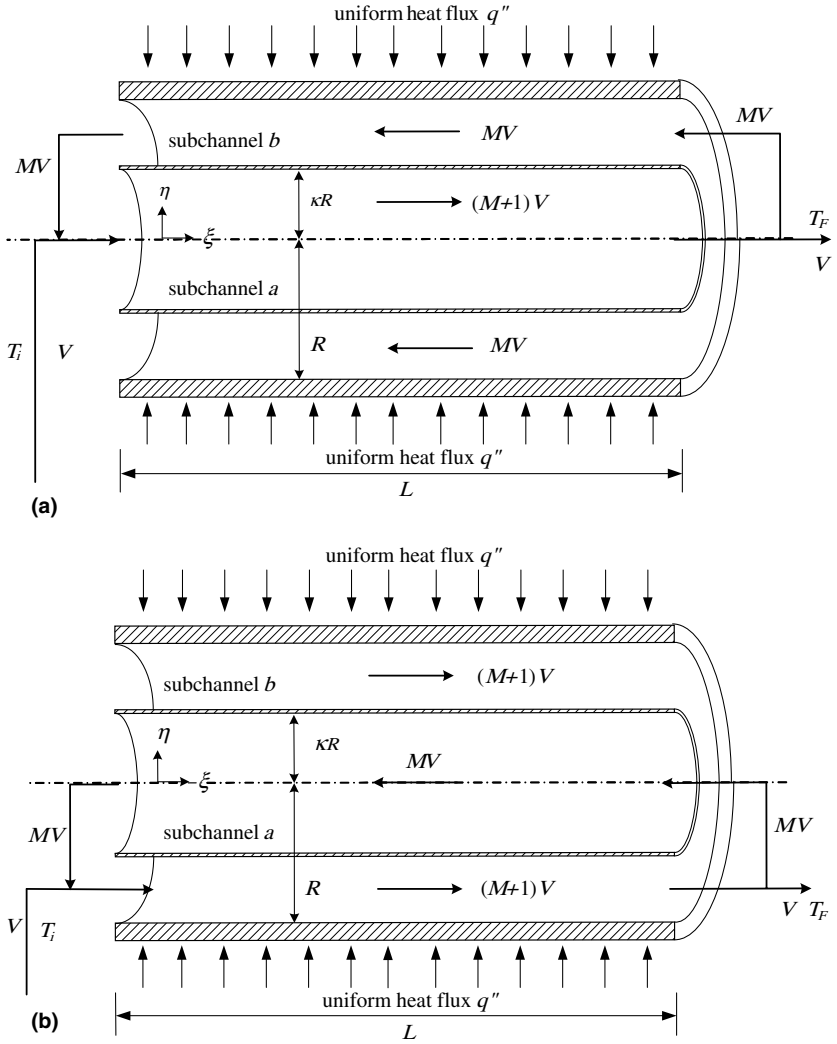

Fig. 1. Schematic diagrams of double-pass concentric circular heat exchangers with external recycle at both ends.

In each flow pattern, the fluid is completely mixed at the inlet and outlet of the tube.

After the following assumptions are made in this analysis: constant physical properties and uniform heat fluxes on the outer tube; fully-developed laminar flow in the entire length in each channel; negligible entrance length, end effects and axial conduction; negligible thickness and thermal resistance in the impermeable sheet, the equations of energy in dimensionless form in terms of temperatures, T_a and T_b, and velocity distributions in the inner channel and annulus, v_a and v_b, may be written as

$$\frac{v_a(\eta)R^2}{\alpha L\,Gz}\frac{\partial\psi_a(\eta,\xi)}{\partial\xi}=\frac{1}{\eta}\left[\frac{\partial}{\partial\eta}\left(\eta\frac{\partial\psi_a(\eta,\xi)}{\partial\eta}\right)\right] \tag{1}$$

$$\frac{v_b(\eta)R^2}{\alpha L\,Gz}\frac{\partial\psi_b(\eta,\xi)}{\partial\xi}=\frac{1}{\eta}\left[\frac{\partial}{\partial\eta}\left(\eta\frac{\partial\psi_b(\eta,\xi)}{\partial\eta}\right)\right] \tag{2}$$

$$v_a(\eta)=2\overline{v_a}\left(1-\left(\frac{\eta}{\kappa}\right)^2\right)\quad 0\leqslant\eta\leqslant\kappa \tag{3}$$

$$v_b(\eta)=\frac{2\overline{v_b}}{W_1}[1-\eta^2+W_2\ln\eta]\quad \kappa\leqslant\eta\leqslant 1 \tag{4}$$

$$\overline{v_a}=\frac{(M+1)V}{\pi(\kappa R)^2}\quad\text{and}\quad\overline{v_b}=-\frac{MV}{\pi R^2-\pi(\kappa R)^2}$$

for Flow Pattern A (5)

$$\overline{v_a}=-\frac{MV}{\pi(\kappa R)^2}\quad\text{and}\quad\overline{v_b}=\frac{(M+1)V}{\pi R^2-\pi(\kappa R)^2}$$

for Flow Pattern B (6)

in which

$$\eta=\frac{r}{R},\quad\xi=\frac{z}{L\cdot Gz},\quad\psi_a=\frac{k(T_a-T_i)}{q''R},$$

$$\psi_b=\frac{k(T_b-T_i)}{q''R},\quad W_1=\left[\frac{1-\kappa^4}{1-\kappa^2}-\frac{1-\kappa^2}{\ln\frac{1}{\kappa}}\right],$$

$$W_2=\left(\frac{1-\kappa^2}{\ln 1/\kappa}\right),\quad Gz=\frac{D}{L}RePr=\frac{4V}{\pi\alpha L} \tag{7}$$

The boundary conditions for solving Eqs. (1) and (2) are

$$\frac{\partial \psi_a(0,\xi)}{\partial \eta} = 0 \tag{8}$$

$$\frac{\partial \psi_b(1,\xi)}{\partial \eta} = 1 \tag{9}$$

$$\frac{\partial \psi_a(\kappa,\xi)}{\partial \eta} = \frac{\partial \psi_b(\kappa,\xi)}{\partial \eta} \tag{10}$$

$$\psi_a(\kappa,\xi) = \psi_b(\kappa,\xi) \tag{11}$$

The technique is introduced that remove the inhomogeneous boundary condition (Eq. (9)) so that they can be treated by extending the method of eigenfunction expansions. The formal solution can be found by linear superposition as follows:

$$\psi_a(\eta,\xi) = \phi_a(\eta,\xi) + \theta_a(\eta,\xi) \tag{12}$$

$$\psi_b(\eta,\xi) = \phi_b(\eta,\xi) + \theta_b(\eta,\xi) \tag{13}$$

2.1. Asymptotic solution of inhomogeneous boundary conditions

$$\frac{v_a(\eta)R^2}{\alpha L\, Gz}\frac{\partial \theta_a(\eta,\xi)}{\partial \xi} = \frac{1}{\eta}\left[\frac{\partial}{\partial \eta}\left(\eta \frac{\partial \theta_a(\eta,\xi)}{\partial \eta}\right)\right] \tag{14}$$

$$\frac{v_b(\eta)R^2}{\alpha L\, Gz}\frac{\partial \theta_b(\eta,\xi)}{\partial \xi} = \frac{1}{\eta}\left[\frac{\partial}{\partial \eta}\left(\eta \frac{\partial \theta_b(\eta,\xi)}{\partial \eta}\right)\right] \tag{15}$$

$$\frac{\partial \theta_a(0,\xi)}{\partial \eta} = 0 \tag{16}$$

$$\frac{\partial \theta_b(1,\xi)}{\partial \eta} = 1 \tag{17}$$

$$\frac{\partial \theta_a(\kappa,\xi)}{\partial \eta} = \frac{\partial \theta_b(\kappa,\xi)}{\partial \eta} \tag{18}$$

$$\theta_a(\kappa,\xi) = \theta_b(\kappa,\xi) \tag{19}$$

The rising of the fluid temperature is linear in ξ with the assumption of the fluid being sufficiently far downstream from the inlet of the heated section. Hence solutions of the following forms of $\theta_a(\eta,\xi)$ and $\theta_b(\eta,\xi)$ seems reasonable

$$\theta_a(\eta,\xi) = a_1\xi + H_a(\eta) \tag{20a}$$

and

$$\theta_b(\eta,\xi) = b_1\left(\frac{1}{Gz} - \xi\right) + H_b(\eta) \tag{20b}$$

for flow pattern A, and

$$\theta_a(\eta,\xi) = a_1\left(\frac{1}{Gz} - \xi\right) + H_a(\eta) \tag{21a}$$

and

$$\theta_b(\eta,\xi) = b_1\xi + H_b(\eta) \tag{21b}$$

in which a_1 and b_1 are constants to be determined presently.

Substituting Eqs. (20) and (21) into Eqs. (14) and (15) and integrating twice of the resultant equations gives

Flow Pattern A

$$\theta_a(\eta,\xi) = a_1\xi + \frac{a_1(M+1)}{2\kappa^4}\left(\frac{\kappa^2}{4}\eta^2 - \frac{\eta^4}{16} + a_2\ln\eta + a_3\right) \tag{22}$$

$$\theta_b(\eta,\xi) = b_1\left(\frac{1}{Gz} - \xi\right) + \frac{b_1 M}{2W_1(1-\kappa^2)} \times \left[\frac{1}{4}\eta^2 - \frac{1}{16}\eta^4 + \frac{W_2}{4}\eta^2(\ln\eta - 1) + b_2\ln\eta + b_3\right] \tag{23}$$

Flow Pattern B

$$\theta_a(\eta,\xi) = a_1\left(\frac{1}{Gz} - \xi\right) + \frac{a_1 M}{2\kappa^4}\left(\frac{\kappa^2}{4}\eta^2 - \frac{\eta^4}{16} + a_2\ln\eta + a_3\right) \tag{24}$$

$$\theta_b(\eta,\xi) = b_1\xi + \frac{b_1(M+1)}{2W_1(1-\kappa^2)} \times \left[\frac{1}{4}\eta^2 - \frac{1}{16}\eta^4 + \frac{W_2}{4}\eta^2(\ln\eta - 1) + b_2\ln\eta + b_3\right] \tag{25}$$

in which a_2, a_3, b_2 and b_3 are integration constants.

2.2. Expansion in terms of eigenfunctions of the homogeneous problem

The functions $\phi_a(\eta,\xi)$ and $\phi_b(\eta,\xi)$ in Eqs. (12) and (13) will be damped out exponentially with ξ and the associated boundary conditions are

$$\frac{\partial \phi_a(0,\xi)}{\partial \eta} = 0 \tag{26}$$

$$\frac{\partial \phi_b(1,\xi)}{\partial \eta} = 0 \tag{27}$$

$$\frac{\partial \phi_a(\kappa,\xi)}{\partial \eta} = \frac{\partial \phi_b(\kappa,\xi)}{\partial \eta} \tag{28}$$

$$\phi_a(\kappa,\xi) = \phi_b(\kappa,\xi) \tag{29}$$

We anticipate that the solutions to the equations for $\phi_a(\eta,\xi)$ and $\phi_b(\eta,\xi)$ will be expanded in terms of the eigenfunctions to obtain an explicit solution

$$\phi_a(\eta,\xi) = \sum_{m=0}^{\infty} S_{a,m}F_{a,m}(\eta)G_m(\xi) \tag{30}$$

$$\phi_b(\eta,\xi) = \sum_{m=0}^{\infty} S_{b,m}F_{b,m}(\eta)G_m(\xi) \tag{31}$$

Applied to the governing equations of $\phi_a(\eta,\xi)$ and $\phi_b(\eta,\xi)$ leads to

$$G_m(\xi) = e^{-\lambda_m\left(\frac{1}{Gz} - \xi\right)} \tag{32}$$

$$F''_{a,m}(\eta) + \frac{F'_{a,m}(\eta)}{\eta} - \frac{v_a(\eta)R^2\lambda_m}{\alpha L\, Gz}F_{a,m}(\eta) = 0 \tag{33}$$

$$F''_{b,m}(\eta) + \frac{F'_{b,m}(\eta)}{\eta} - \frac{v_b(\eta)R^2\lambda_m}{\alpha L\, Gz}F_{b,m}(\eta) = 0 \tag{34}$$

and also the boundary conditions in Eqs. (26)–(29) can be rewritten as

$$F'_{a,m}(0) = 0 \tag{35}$$

$$F'_{b,m}(1) = 0 \tag{36}$$

$$S_{a,m}F'_{a,m}(\kappa) = S_{b,m}F'_{b,m}(\kappa) \tag{37}$$

$$S_{a,m}F_{a,m}(\kappa) = S_{b,m}F_{b,m}(\kappa) \tag{38}$$

combination of Eqs. (37) and (38) yields

$$\frac{F'_{a,m}(\kappa)}{F_{a,m}(\kappa)} = \frac{F'_{b,m}(\kappa)}{F_{b,m}(\kappa)} \tag{39}$$

in which the eigenfunctions $F_{a,m}(\eta)$ and $F_{b,m}(\eta)$ are assumed to be polynomials to avoid the loss of generality. With Eqs. (35) and (36), we have

$$F_{a,m}(\eta) = \sum_{n=0}^{\infty} d_{mn}\eta^n, \quad d_{m0} = 1 \text{ (selected)}, \quad d_{m1} = 0 \tag{40}$$

$$F_{b,m}(\eta) = \sum_{n=0}^{\infty} e_{mn}\eta^n, \quad d_{m0} = 1 \text{ (selected)}, \quad d_{m1} = 0 \tag{41}$$

Substituting Eqs. (40) and (41) into Eqs. (33) and (34), all the coefficients d_{mn} and e_{mn} may be expressed in terms of λ_m, as referred to in Appendix A, and the eigenfunctions associated with the corresponding eigenvalues are also well defined by Eqs. (40) and (41). The mathematical treatment is similar to that in the previous work [21] with the orthogonality conditions when $n \neq m$ as follows:

$$\int_0^{\kappa} \left[\frac{v_a \cdot R^2}{L \cdot \alpha \cdot Gz}\right] S_{a,m}S_{a,n}\eta F_{a,m}F_{a,n}\,d\eta + \int_{\kappa}^{1} \left[\frac{v_b \cdot R^2}{L \cdot \alpha \cdot Gz}\right] S_{b,m}S_{b,n}\eta F_{b,m}F_{b,n}\,d\eta = 0 \tag{42}$$

2.3. Complete solution of double-pass concentric tubes with recycle

Substitution of Eqs. (22), (23) for flow pattern A (or Eqs. (24), (25) for flow pattern B) and Eqs. (30), (31) with the use of boundary conditions Eqs. (8)–(11) give a set of simultaneous equations to solve the constants a_1, a_2 and a_3 for subchannel a and b_1, b_2 and b_3 for subchannel b as follows:

$$a_2 = 0 \tag{43}$$

$$\frac{b_1 M}{8(1-\kappa^2)W_1} + [(1 - W_2) + b_2] = 1 \tag{44}$$

$$S_{a,m}F'_{a,m}(\kappa)G_m(\xi) + \frac{a_1(M+1)}{8\kappa} = S_{b,m}F'_{b,m}(\kappa)G_m(\xi) + \frac{b_1 M}{4(1-\kappa^2)W_1} \times \left(\kappa - \frac{1}{2}\kappa^3 + W_2\left(\kappa\ln\kappa - \frac{1}{2}\kappa\right) + \frac{b_2}{\kappa}\right) \tag{45}$$

$$S_{a,m}F_{a,m}(\eta)G_m(\xi) + a_1\xi + \frac{a_1(M+1)}{2\kappa^4}\left(\frac{3\kappa^4}{16} + a_2\ln\kappa + a_3\right) = S_{b,m}F_{b,m}(\eta)G_m(\xi) + b_1\left(\frac{1}{Gz} - \xi\right) + \frac{b_1 M}{2W_1(1-\kappa^2)} \times \left[\frac{1}{4}\kappa^2 - \frac{1}{16}\kappa^4 + \frac{W_2}{4}\kappa^2(\ln\kappa - 1) + b_2\ln\kappa + b_3\right] \tag{46}$$

for flow pattern A, and

$$a_2 = 0 \tag{47}$$

$$\frac{b_1(M+1)}{8(1-\kappa^2)W_1} + [(1 - W_2) + b_2] = 1 \tag{48}$$

$$S_{a,m}F'_{a,m}(\kappa)G_m(\xi) + \frac{a_1 M}{8\kappa} = S_{b,m}F'_{b,m}(\kappa)G_m(\xi) + \frac{b_1(M+1)}{4(1-\kappa^2)W_1} \times \left(\kappa - \frac{1}{2}\kappa^3 + W_2\left(\kappa\ln\kappa - \frac{1}{2}\kappa\right) + \frac{b_2}{\kappa}\right) \tag{49}$$

$$S_{a,m}F_{a,m}(\eta)G_m(\xi) + a_1\left(\frac{1}{Gz} - \xi\right) + \frac{a_1 M}{2\kappa^4}\left(\frac{3\kappa^4}{16} + a_2\ln\kappa + a_3\right) = S_{b,m}F_{b,m}(\eta)G_m(\xi) + b_1\xi + \frac{b_1(M+1)}{2W_1(1-\kappa^2)} \times \left[\frac{1}{4}\kappa^2 - \frac{1}{16}\kappa^4 + \frac{W_2}{4}\kappa^2(\ln\kappa - 1) + b_2\ln\kappa + b_3\right] \tag{50}$$

Accordingly, once all the constants in Eqs. (22) and (23) for flow pattern A (or Eqs. (24), (25) for flow pattern B) and Eqs. (30), (31) were obtained, the dimensionless inlet and outlet temperatures for double-pass operations were thus obtained in terms of the Graetz number (Gz), eigenvalues ($\lambda_{a,m}$ and $\lambda_{b,m}$), expansion coefficients ($S_{a,m}$ and $S_{b,m}$), the location of the impermeable sheet (κ) and eigenfunctions ($F_{a,m}(\eta_a)$ and $F_{b,m}(\eta_b)$). The dimensionless outlet temperature ψ_F is referred to as the bulk temperature, may be calculated

$$\psi_F = \frac{\int_0^{\kappa} v_a 2\pi R^2 \eta\psi_a\left(\eta, \frac{1}{Gz}\right)d\eta}{V(M+1)} = \frac{1}{(M+1)}\left\{8\sum_{m=0}^{\infty}\frac{S_{a,m}}{\lambda_m}[\kappa \cdot F'_{a,m}(\kappa)] - \int_0^{\kappa}\frac{-4(M+1)}{W_1(1-\kappa^2)}\left(1 - \left(\frac{\eta}{\kappa}\right)^2\right)\eta\theta_a\left(\eta, \frac{1}{Gz}\right)d\eta\right\} \tag{51}$$

or

$$\psi_F = \frac{-\int_{\kappa}^{1} v_b 2\pi R^2 \psi_{b,m}\left(\eta, \frac{1}{Gz}\right)d\eta}{VM} = \frac{1}{M}\left\{-8\sum_{m=0}^{\infty}\frac{S_{b,m}}{\lambda_m}[-\kappa \cdot F'_{b,m}(\kappa)] - \int_0^{\kappa}\frac{-4M}{W_1(1-\kappa^2)}(1 - \eta^2 + W_2 \cdot \ln\eta)\eta\theta_b\left(\eta, \frac{1}{Gz}\right)d\eta\right\} \tag{52}$$

for the flow pattern A, and

$$\psi_F = \frac{-\int_0^{\kappa} v_a 2\pi R^2 \eta\psi_a\left(\eta, \frac{1}{Gz}\right)d\eta}{VM} = \frac{1}{M}\left\{-8\sum_{m=0}^{\infty}\frac{S_{a,m}}{\lambda_m}[\kappa \cdot F'_{a,m}(\kappa)] - \int_0^{\kappa}\frac{-4M}{W_1(1-\kappa^2)}\left(1 - \left(\frac{\eta}{\kappa}\right)^2\right)\eta\theta_a\left(\eta, \frac{1}{Gz}\right)d\eta\right\} \tag{53}$$

or

$$\psi_F = \frac{\int_\kappa^1 v_b 2\pi R^2 \psi_{b,m}\left(\eta,\frac{1}{Gz}\right)d\eta}{V(M+1)} = \frac{1}{(M+1)}\left\{8\sum_{m=0}^{\infty}\frac{S_{b,m}}{\lambda_m}[-\kappa\cdot F'_{b,m}(\kappa)] + \int_0^\kappa \frac{4(M+1)}{W_1(1-\kappa^2)}(1-\eta^2+W_2\cdot\ln\eta)\eta\theta_b\left(\eta,\frac{1}{Gz}\right)d\eta\right\} \quad (54)$$

for flow pattern B, and may be examined using Eq. (55) which is readily obtained from the following overall energy balance in the outer tube

$$\rho C_p V(T_F - T_i) = \int_0^L q''(2\pi R)\,dz \quad (55)$$

or

$$\psi_F = \frac{8}{Gz} \quad (56)$$

In Eq. (55) the left-hand side refers to the net outlet energy while the right-hand side is the total amount of heat transfer from the outer tube into the fluid. The dimensionless mixed inlet temperature is calculated after the coefficients, $S_{a,m}$ and $S_{b,m}$, are obtained as follows:

$$\psi_a(\eta,0) = \frac{-\int_\kappa^1 v_b 2\pi R^2\eta\psi_b(\eta,0)\,d\eta + V\cdot 0}{V(M+1)} = \frac{1}{(M+1)}\left\{-8\sum_{m=0}^{\infty}\frac{e^{\frac{-\lambda_m}{Gz}}S_{b,m}}{\lambda_m}[-\kappa\cdot F'_{b,m}(\kappa)] - \int_0^\kappa \frac{-4M}{W_1(1-\kappa^2)}(1-\eta^2+W_2\cdot\ln\eta)\eta\theta_b(\eta,0)\,d\eta\right\} \quad (57)$$

for flow pattern A. Similarly, for flow pattern B

$$\psi_b(\eta,0) = \frac{-\int_0^\kappa v_a 2\pi R^2\eta\psi_a(\eta,0)\,d\eta + V\cdot 0}{V(M+1)} = \frac{1}{(M+1)}\left\{8\sum_{m=0}^{\infty}\frac{e^{\frac{-\lambda_m}{Gz}}S_{a,m}}{\lambda_m}[-\kappa\cdot F'_{a,m}(\kappa)] + \int_0^\kappa \frac{-4M}{W_1(1-\kappa^2)}\left(1-\left(\frac{\eta}{\kappa}\right)^2\right)\eta\theta_a(\eta,0)\,d\eta\right\} \quad (58)$$

2.4. Single-pass devices without recycle

For a single-pass operation of the same size without recycle, that is, the impermeable tube in Fig. 1(a) and (b) is removed, and thus $\kappa = 1$ and 0, respectively. The velocity distribution and equation of energy in dimensionless form may be written as

$$\frac{v_0(\eta)R^2}{\alpha L\,Gz}\frac{\partial\psi_0(\eta,\xi)}{\partial\xi} = \frac{1}{\eta}\left[\frac{\partial}{\partial\eta}\left(\eta\frac{\partial\psi_0(\eta,\xi)}{\partial\eta}\right)\right] \quad (59)$$

$$v_0(\eta) = \frac{2V}{\pi R^2}(1-\eta^2) \quad 0 \leqq \eta \leqq 1 \quad (60)$$

$$\eta = \frac{r}{R}, \quad \xi = \frac{z}{L\cdot Gz}, \quad \psi_0 = \frac{k(T_0 - T_i)}{q''R}, \quad Gz = \frac{4V}{\alpha\pi L} \quad (61)$$

The initial and boundary conditions for solving Eq. (59) are

$$\frac{\partial\psi_0(0,\xi)}{\partial\eta} = 0 \quad (62)$$

$$\frac{\partial\psi_0(1,\xi)}{\partial\eta} = 1 \quad (63)$$

$$\psi_0(\eta,0) = 0 \quad (64)$$

The calculation procedure for a single-pass operation is rather simpler than that for double-pass ones in the previous section by linear superposition as follows:

$$\psi_0(\eta,\xi) = \phi_0(\eta,\xi) + \theta_0(\eta,\xi) \quad (65)$$

$$\theta_0(\eta,\xi) = c_1\xi + H_0(\eta) \quad (66)$$

$$\phi_0(\eta,\xi) = \sum_{m=0}^{\infty} S_{0,m}F_{0,m}(\eta)G_m(\xi) \quad (67)$$

The result gives the asymptotic solution and of the dimensionless temperature as a function of the dimensionless radial and axial coordinates

$$\theta_0(\eta,\xi) = 8\xi + \eta^2 - \frac{1}{4}\eta^4 - \frac{7}{24} \quad (68)$$

while the homogeneous part, Eq. (67), of the dimensionless outlet temperature for a single-pass operation ($\theta_{0,F}$) was evaluated in terms of the Graetz number (Gz), eigenvalues ($\lambda_{0,m}$), expansion coefficient ($S_{0,m}$) and eigenfunctions ($F_{0,m}(\eta)$) as follows:

$$\psi_{0,F} = \frac{\int_0^1 v_0 2\pi R^2\eta\psi_0(\eta,1)\,d\eta}{V} = \left\{8\sum_{m=0}^{\infty}\frac{S_{0,m}}{\lambda_m}[-F'_{0,m}(1)] + \int_0^\kappa \frac{4}{W_1(1-\kappa^2)}(1-\eta^2+W_2\cdot\ln\eta)\eta\theta_0\left(\eta,\frac{1}{Gz}\right)d\eta\right\} \quad (69)$$

and may be examined using Eq. (70), which is readily obtained from the following overall energy balance in the outer tube

$$q''(2\pi Rz) = \int_0^{2\pi}\int_0^R \rho C_p(T - T_i)v_z r\,dr\,d\theta \quad (70)$$

or

$$\xi = \frac{1}{2}\int_0^1 \theta_0(\eta,\xi)(1-\eta^2)\eta\,d\eta \quad (71)$$

3. Heat-transfer efficiency improvement

The average Nusselt number for double-pass operations with recycle may be defined as

$$\overline{Nu} = \frac{\bar{h}(2R)}{k} = \frac{\bar{h}D}{k} \tag{72}$$

and the average heat transfer coefficient is defined as

$$\begin{aligned} q''(2\pi RL) &= V\rho C_p(T_F - T_i) \\ &= \bar{h}(2\pi RL)[\overline{T_w} - (T_F + T_i)/2] \end{aligned} \tag{73}$$

in which

$$\overline{T_w} = \frac{\int_0^L T_w(R,z)\,dz}{L} \tag{74}$$

or

$$\begin{aligned} \bar{h} &= \frac{V\rho C_p(T_F - T_i)}{\pi RL(2\overline{T_w} - T_F - T_i)} \\ &= \frac{V\rho C_p(T_F - T_i)}{\pi RL[2(\overline{T_w} - T_i) - (T_F - T_i)]} \end{aligned} \tag{75}$$

thus

$$\begin{aligned} \overline{Nu} &= \frac{Gz\cdot\psi_F}{\left(4Gz\cdot\int_0^{1/Gz}\psi_w\,d\xi\right) - 2\psi_F} \\ &= \frac{Gz\cdot\psi_F}{\left(4Gz\cdot\int_0^{1/Gz}\psi_b(1,\xi)\,d\xi\right) - 2\psi_F} \end{aligned} \tag{76}$$

Similarly, for a single-pass operation

$$\begin{aligned} \overline{Nu_0} &= \frac{Gz\cdot\psi_{0,F}}{\left(4Gz\cdot\int_0^{1/Gz}\psi_{0,w}\,d\xi\right) - 2\psi_{0,F}} \\ &= \frac{Gz\cdot\psi_{0,F}}{\left(4Gz\cdot\int_0^{1/Gz}\psi_{0,b}(1,\xi)\,d\xi\right) - 2\psi_{0,F}} \end{aligned} \tag{77}$$

Based on a single-pass operation, the device performance improvement by employing a double-pass operation with recycle is best illustrated by calculating the percent increase in heat-transfer rate, based on the heat-transfer rate of single-pass operations without recycle of the same working dimensions and operating conditions as

$$I_h = \frac{\overline{Nu} - \overline{Nu_0}}{\overline{Nu_0}} = \frac{4Gz\cdot\int_0^{1/Gz}\psi_{0,b}(1,\xi)\,d\xi - 2\psi_{0,F}}{4Gz\cdot\int_0^{1/Gz}\psi_b(1,\xi)\,d\xi - 2\psi_F} - 1 \tag{78}$$

4. Results and discussion

The energy equation of laminar counterflow concentric circular heat exchangers with external recycle under uniform wall fluxes was developed theoretically. The complete solution was found theoretically by linear superposition by using the asymptotic solution inhomogeneous boundary conditions and the orthogonal expansion technique with the eigenfunctions of the related homogeneous problem. Table 1 illustrates the dominant eigenvalue and their associated expansion coefficients in calculating the Nusselt number for $\kappa = 0.7$, $M = 5$ and $Gz = 1$, 10, 100 and 1000. The results in Table 1 show that only the first negative eigenvalue is needed during the calculation procedure due to the rapid convergence.

4.1. Heat transfer efficiency in double-pass devices of flow pattern A

Comparisons of dimensionless wall temperatures, $\psi_b(1,\xi)$ and $\psi_0(1,\xi)$, as well as average Nusselt number, $\overline{Nu}$ and $\overline{Nu_0}$, were calculated and represented in Figs. 2–4. Fig. 2 shows that another more practical form of mixed dimensionless inlet temperature $\overline{\psi_a}(0)$ vs. Gz with recycle ratio M and subchannel thickness ratio κ as parameters while Fig. 3 for the theoretical average Nusselt number $\overline{Nu}$ and $\overline{Nu_0}$ vs. Gz with κ and M as parameters. The mixed dimensionless inlet temperature increases with the amount of the recycle fluid (or recycle ratio) for the dimensionless outlet temperature kept at $\psi_F = 8/Gz$, as shown in Eq. (56), and hence the mixed dimensionless inlet temperature increases with the amount of the recycle fluid (or recycle ratio). Accordingly, it is shown in Fig. 2 that the dimensionless inlet temperature of fluid after mixing the recycle fluid increases with recycle ratio and with decreasing subchannel thickness ratio but decreases with Graetz number. The application of the recycle-effect concept to heat exchangers creates two conflicting effects: the desirable effect of increasing convective heat-transfer coefficient and the undesirable effect of decreasing temperature gradient. The desirable effect of convective heat-transfer

Table 1
Eigenvalues and expansion coefficients as well as average Nusselt number in double-pass devices (Flow pattern A) for $\kappa = 0.7$ and $M = 5$

Gz	m	λ_m	$S_{a,m}$	$S_{b,m}$	a_1	a_2	a_3	b_1	b_2	b_3	$\overline{Nu}(\lambda_1)$	$\overline{Nu}(\lambda_1,\lambda_2)$
1	1	−0.82	-5.9×10^{-16}	-1.1×10^{-18}	1.36	0	0.37	−0.03	−0.33	−3.36	0.25	0.25
	2	−2.40	6.8×10^{-17}	6.2×10^{-24}	1.36	0	0.37	−0.03	−0.33	−3.36		
10	1	−0.82	8.3×10^{-16}	-8.6×10^{-18}	0.07	0	0.84	1.51	0.12	0.18	2.01	2.01
	2	−2.40	-3.3×10^{-15}	-1.9×10^{-22}	0.07	0	0.84	1.51	0.12	0.18		
100	1	−0.82	5.4×10^{-16}	5.4×10^{-16}	−0.08	0	−0.10	1.70	0.12	0.17	9.91	9.91
	2	−2.40	-7.3×10^{-15}	-4.1×10^{-22}	−0.08	0	−0.10	1.70	0.12	0.17		
1000	1	−0.82	-1.1×10^{-15}	2.2×10^{-15}	−0.10	0	−0.02	1.72	0.12	0.17	16.44	16.44
	2	−2.40	-3.2×10^{-15}	-1.9×10^{-22}	−0.10	0	−0.02	1.72	0.12	0.17		

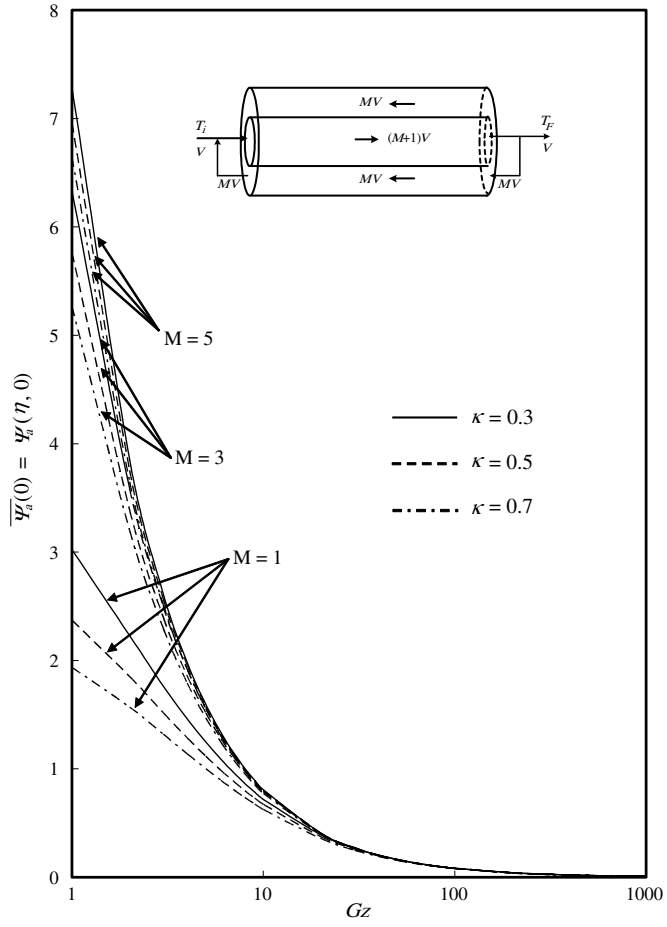

Fig. 2. Dimensionless inlet bulk temperatures of fluid after mixing vs. Gz with κ and M as parameters (flow pattern A).

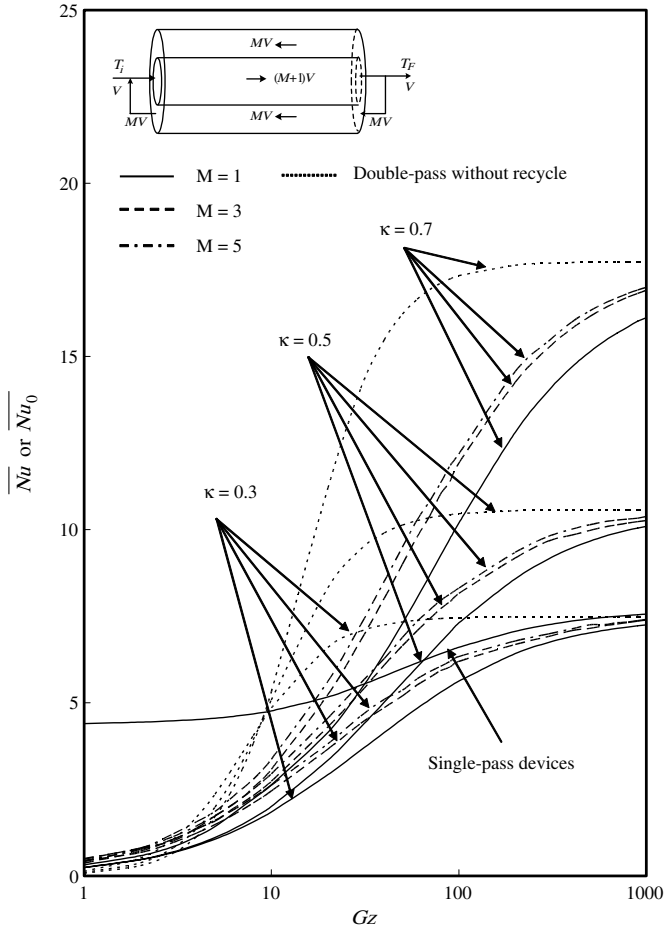

Fig. 3. Theoretical average Nusselt number vs. Gz with κ and M as parameters (flow pattern A).

coefficient increases when the recycle ratio, channel thickness ratio and Graetz number rise. The reason why the desirable effect increases with increasing the channel thickness ratio κ may be considered as that the enhancement of convective heat-transfer rate due to increasing the flow velocity in the annular channel, where the fluid is heated, is more effective than that in the inner channel. Consequently, the increment of the convective heat-transfer coefficient can compensate the decrement of the undesirable effect of decreasing temperature gradient to make the dimensionless outlet temperature equal to $\psi_F = 8/Gz$. It is also found that the same tendency of change of the average Nusselt number $\overline{Nu}$ and $\overline{Nu_0}$ for both devices with and without recycle as shown in Fig. 3. It is concluded that the theoretical average Nusselt number increases with increasing the channel thickness ratio κ, Graetz number Gz and recycle ratio M. On the other hand, $(\overline{Nu} - \overline{Nu_0})$ increases with increasing Gz and κ, but the increase with Gz is limited as Gz approaches infinite. The higher convective heat-transfer coefficient, the larger heat removed on the outer wall for a fixed outlet temperature. Hence, it yields in a lower wall temperature along the axis as shown in Fig. 4.

Some theoretical predictions of the improvement in device performance I_h were given in Table 2. The minus signs in Table 2 indicate that no improvement in heat transfer efficiency can be achieved as the channel thickness ratio κ greater than 0.3 and the Graetz number larger than some values, say $Gz > 60$, and in this case, the single-pass device is preferred to be employed rather than using the double-pass one operating at such conditions.

4.2. Improvement in heat transfer efficiency of flow pattern B

The calculation procedures performed in flow pattern B are similar to those in the previous section of flow pattern A except that it is in reverse flow direction. Since the position of the impermeable sheet has significant influence on the heat transfer behavior, the theoretical average Nusselt number $\overline{Nu}$ and $\overline{Nu_0}$ was calculated and presented in Fig. 5 with Graetz number Gz and channel thickness ratio κ as parameters while the percentages of the heat-transfer efficiency improvement were shown in Table 3 with Graetz number, recycle ratio and subchannel thickness ratio as parameters. Fig. 5 shows that the theoretical average Nusselt number increase with increasing Graetz number Gz, and subchannel thickness ratio κ but decreases with increasing recycle ratio M. Table 3 indicates that the percentages of the heat-transfer efficiency improvement

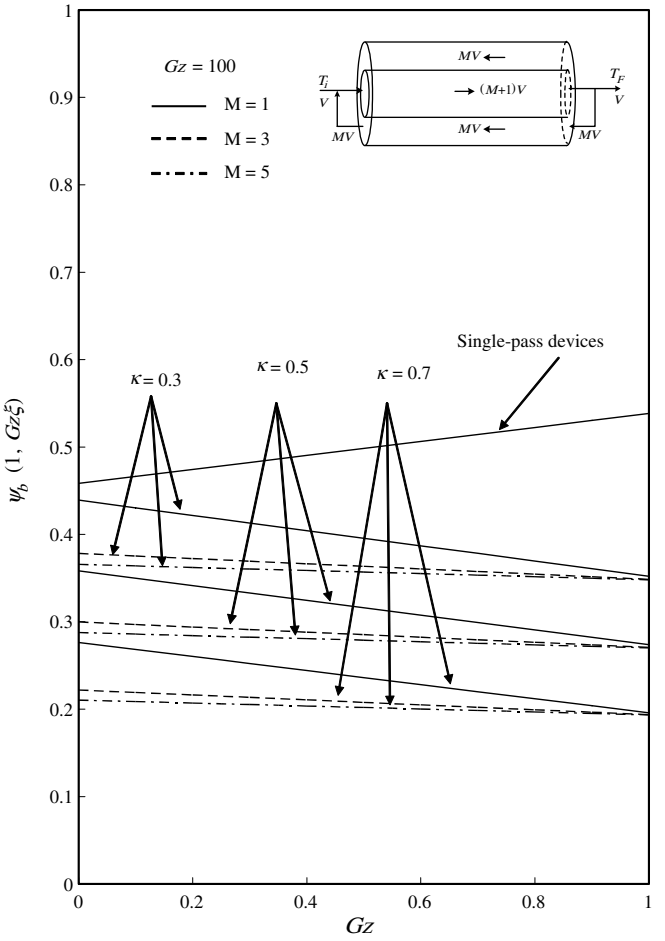

Fig. 4. Dimensionless wall temperatures vs. $Gz\,\xi$ with κ and M as parameters (flow pattern A).

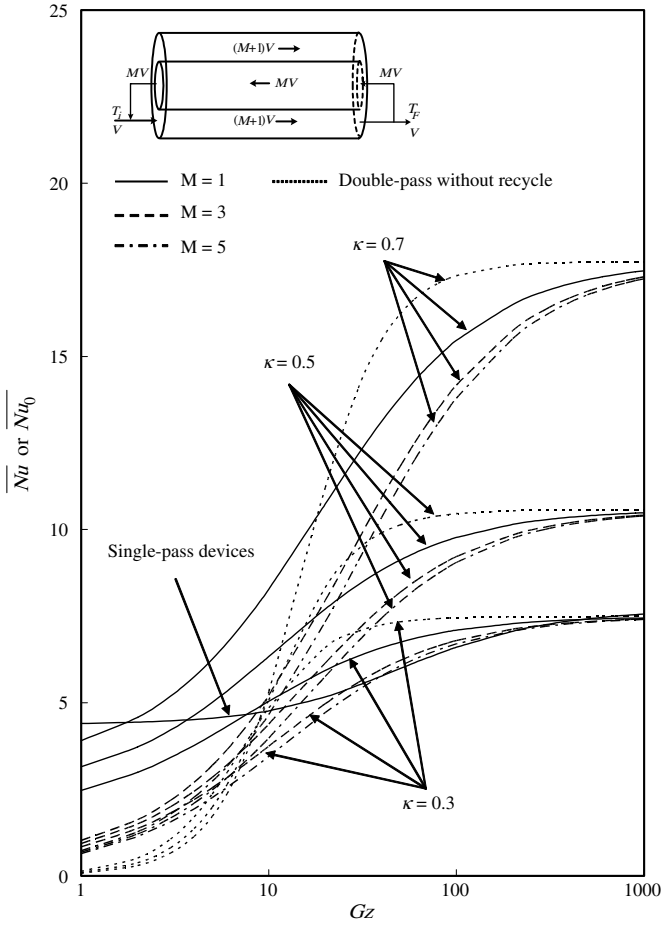

Fig. 5. Theoretical average Nusselt number vs. Gz with κ and M as parameters (flow pattern B).

Table 2
The heat-transfer efficiency improvement with the recycle ratio and subchannel thickness ratio as parameters (flow pattern A)

I_h (%)	$M = 1$			$M = 3$			$M = 5$		
	κ			κ			κ		
	0.3	0.5	0.7	0.3	0.5	0.7	0.3	0.5	0.7
$Gz = 1$	−94.5	−94.5	−92.8	−90.2	−89.0	−91.7	−89.9	−88.6	−90.8
10	−61.3	−58.0	−44.8	−48.6	−42.6	−35.4	−45.1	−38.1	−29.3
100	−14.8	10.7	54.4	−6.1	23.5	80.5	−4.0	25.9	84.6
1000	−4.1	33.6	113.3	−2.3	35.8	123.7	−2.0	37.3	124.9

Table 3
The heat-transfer efficiency improvement with the recycle ratio and subchannel thickness ratio as parameters (flow pattern B)

I_h (%)	$M = 1$			$M = 3$			$M = 5$		
	κ			κ			κ		
	0.3	0.5	0.7	0.3	0.5	0.7	0.3	0.5	0.7
$Gz = 1$	−44.0	−28.4	−11.3	−80.9	−78.8	−76.8	−85.3	−84.4	−83.6
10	5.9	33.1	73.7	−21.4	−8.0	9.6	−27.6	−16.5	−2.2
100	7.4	48.0	134.2	2.9	39.6	114.6	1.5	37.0	108.9
1000	−1.4	38.7	131.2	−1.9	37.8	128.9	−2.0	37.6	128.1

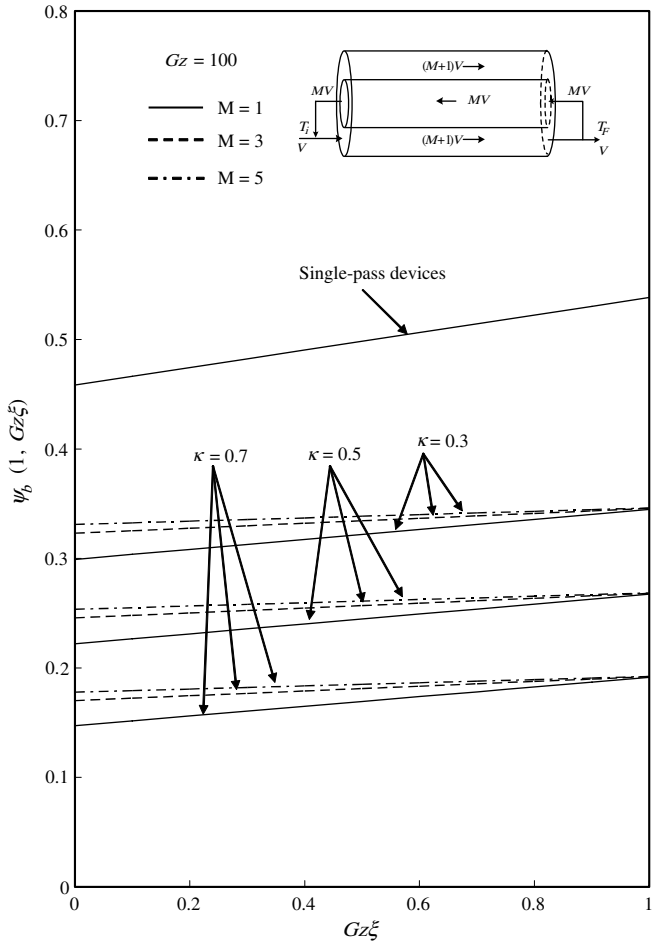

Fig. 6. Dimensionless wall temperatures vs. $Gz\,\xi$ with κ and M as parameters (flow pattern B).

increase with increasing subchannel thickness ratio κ but decrease with increasing recycle ratio M. Meanwhile, the lower wall temperature compared to flow pattern A is obtained, if the flow pattern B is used instead of the flow pattern A, as shown in Figs. 4 and 6. Moreover, at a specific Graetz number, an optimal heat-transfer efficiency improvement may be observed from Table 3.

4.3. Power consumption increment

The friction loss only the friction losses to the walls were significant is assumed and may be estimated using

$$h_{\mathrm{f}} = 4f \cdot \frac{L}{D} \cdot \frac{\bar{v}^2}{2g_{\mathrm{c}}} \tag{79}$$

Table 4
The power consumption increment with subchannel thickness ratio as a parameter (flow pattern A)

M	I_{p}		
	$\kappa = 0.3$	$\kappa = 0.5$	$\kappa = 0.7$
1	495	68	37
3	1994	303	261
5	4499	708	693

Table 5
The power consumption increment with subchannel thickness ratio as a parameter (flow pattern B)

M	I_{p}		
	$\kappa = 0.3$	$\kappa = 0.5$	$\kappa = 0.7$
1	131	36	90
3	1145	228	385
5	3166	591	887

The friction loss in a single-pass operation conduit is calculated using the appropriate equations and working dimensions as follows: $L = 1.2$ m, $R = 0.2$ m, $V = 1 \times 10^{-4}$ m^3/s, $\rho = 997.08$ kg/m^3, $\mu = 8.94 \times 10^{-4}$ kg/m s, and $P_0 = V\rho h_{\mathrm{f},0} = 1.71 \times 10^{-8}$, $W = 2.29 \times 10^{-11}$ hp in a single-pass device. Accordingly, the power consumption increment, I_{p}, due to the friction losses for double-flow operations can be readily derived as

$$I_{\mathrm{p}} = \frac{P - P_0}{P_0} = \frac{V\rho[(M+1)h_{\mathrm{f,a}} + Mh_{\mathrm{f,b}}] - V\rho h_{\mathrm{f},0}}{V\rho h_{\mathrm{f},0}} = \frac{(M+1)^2}{\kappa^4} + \frac{M^2}{(1-\kappa^2)(1-\kappa)^2} - 1 \tag{80}$$

for flow pattern A, and

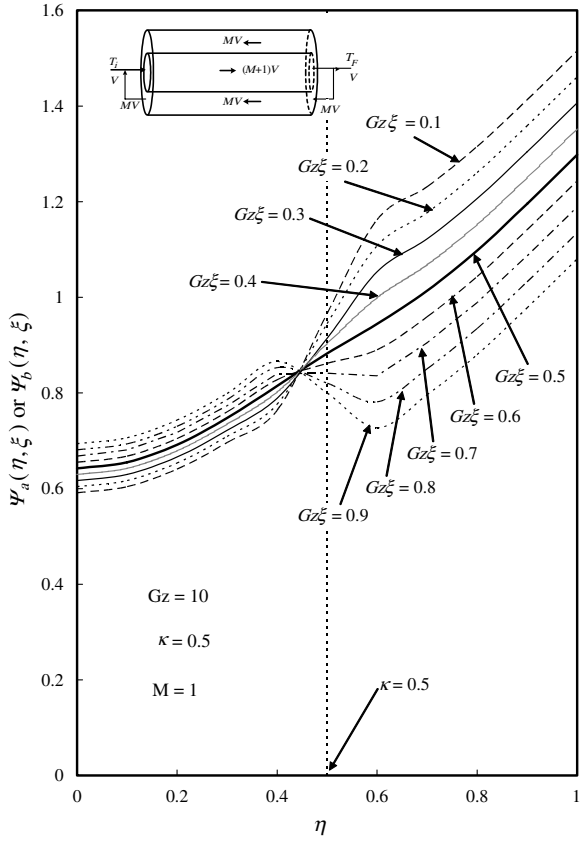

Fig. 7. The local transversal temperature in channels a and b for $Gz = 10$, $\kappa = 0.5$ and $M = 1$, and for various axial distance $Gz\,\xi$ (flow pattern A).

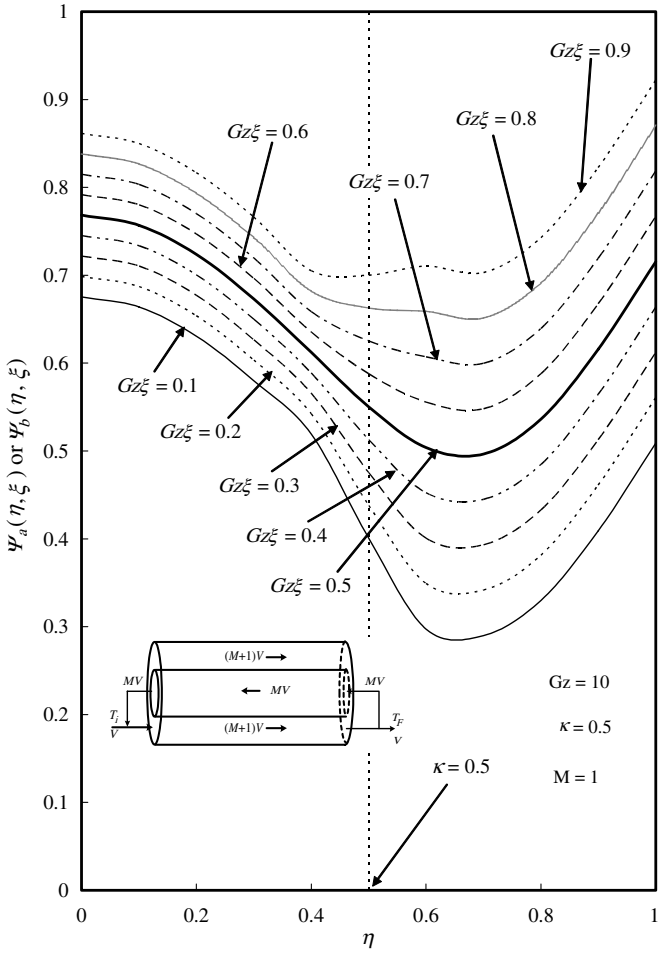

Fig. 8. The local transversal temperature in channels a and b for $Gz = 10$, $\kappa = 0.5$ and $M = 1$, and for various axial distance $Gz\,\xi$ (flow pattern B).

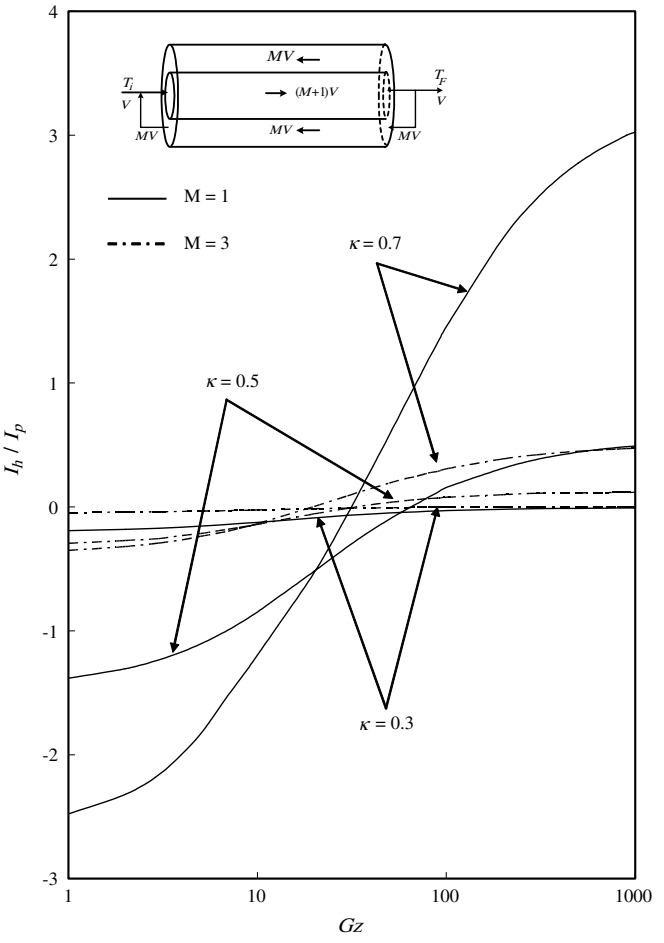

Fig. 9. The values of I_h/I_p vs. Gz with κ and M as parameters (flow pattern A).

$$I_p = \frac{P - P_0}{P_0} = \frac{V\rho[Mh_{f,a} + (M+1)h_{f,b}] - V\rho h_{f,0}}{V\rho h_{f,0}} = \frac{M^2}{\kappa^4} + \frac{(M+1)^2}{(1-\kappa^2)(1-\kappa)^2} - 1 \quad (81)$$

for flow pattern B, respectively.

Some numerical results for I_p for double-pass devices are presented in Tables 4 and 5 for flow pattern A and flow pattern B, respectively. From those tables the power consumption increment does not depend on the Graetz number but increases with decreasing κ for flow pattern A and as κ moves away from 0.5, especially for $\kappa < 0.5$ in flow pattern B. Although the power consumption increment in double-pass operations may be as large as 4499 for $\kappa = 0.3$, the power consumption in the single-pass device is extremely small as $P_0 = V\rho h_{fs,0} = 2.29 \times 10^{-11}$ hp. The power consumption in all devices may be ignored.

5. Conclusions

The theoretical study of laminar counterflow concentric circular heat exchangers under uniform wall fluxes and external recycle has been investigated, and the analytical solution of such conjugated Graetz problems was solved by using the orthogonal expansion technique to expand the eigenfunction in terms of an extended power series. As an illustration the performance of improved device with external recycle, the heat transfer rate in a single-pass device of the same working dimension has also been evaluated for comparisons. The application of the recycle-effect concept in a circular tube can enhance heat transfer rate (and hence lower the maximum wall temperature) of fluid flowing through double-pass heat exchangers by inserting an impermeable sheet with negligible thermal resistance, as indicated from Figs. 3 and 5 and Tables 2 and 3. With those comparisons those figures and tables, the advantage of the present devices is evident for $Gz > 50$ and $Gz > 30$ in flow patterns A and B, respectively. Figs. 3 and 5 illustrate some calculated results of a double-pass device without recycle with the same parameter values for comparisons. With those comparisons, the advantages of both present flow patterns are evident with small Graetz number. The local transversal temperature profiles in subchannels a and b for $Gz = 10$, $\kappa = 0.5$ and $M = 1$, and for various axial distance $Gz\,\xi$ presented in Figs. 7 and 8,

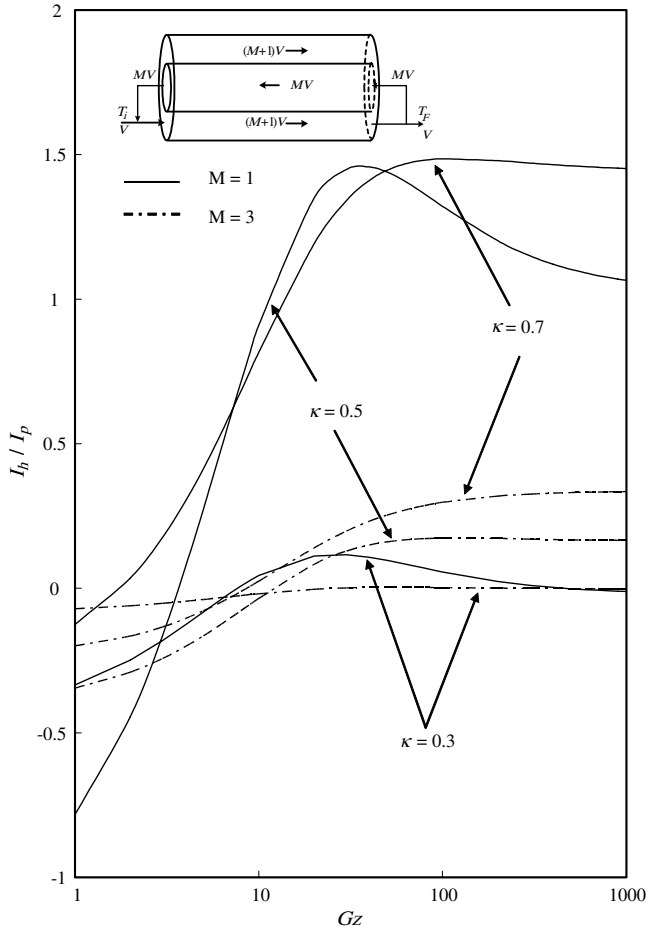

Fig. 10. The values of I_h/I_p vs. Gz with κ and M as parameters (flow pattern B).

respectively, lend credibility to the theoretical predictions of the mathematical formulation. A comparison of Figs. 3 and 5 with Tables 2 and 3 indicates an enhancement of heat transfer rate occurs for flow pattern B with design and operating parameters.

Considerable improvement in heat transfer rate is obtained if the heat exchanger is operated with external recycle in which the enhancement of convective heat-transfer coefficient is provided. However, the evaluation of economic sense including the operating cost in the double-pass heat exchangers with recycle, both the heat transfer improvement I_h and the power consumption increment I_p, which is presented here in the form I_h/I_p, were taken into account in economical feasibility to suitably select the design parameter (κ) and the operating parameters (Gz and M). The results of I_h/I_p with subchannel thickness ratio and recycle ratio as parameters were shown in Figs. 9 and 10 for flow patterns A and B, respectively. Fig. 9 shows that the values of I_h/I_p increase with increasing the subchannel thickness ratio κ and with decreasing the recycle ratio M for flow pattern A while Fig. 10 shows that there exits an economical feasibility, say an optimal I_h/I_p value, in operating double-pass concentric circular heat exchangers in flow pattern B.

Acknowledgement

The authors wish to thank the National Science Council of the Republic of China for its financial support.

Appendix A

Eqs. (33) and (34) can be rewritten as

$$F''_{a,m}(\eta)+\frac{F'_{a,m}(\eta)}{\eta}-\frac{\lambda_m}{2\kappa^2}\left[1-\left(\frac{\eta}{\kappa}\right)^2\right]F_{a,m}(\eta)=0 \tag{A.1}$$

$$F''_{b,m}(\eta)+\frac{F'_{b,m}(\eta)}{\eta}+\frac{\lambda_m}{2W_1(1-\kappa^2)}(1-\eta^2+W_2\cdot\ln\eta)F_{b,m}(\eta)=0 \tag{A.2}$$

in which $W_1=\left[\frac{1-\kappa^4}{1-\kappa^2}-\frac{1-\kappa^2}{\ln\frac{1}{\kappa}}\right]$, $W_2=\left(\frac{1-\kappa^2}{\ln\frac{1}{\kappa}}\right)$ and the term $\ln\eta$ in velocity distributions can be expressed in terms of Taylor's series as follows:

$$\ln\eta=(\eta-1)-\frac{(\eta-1)^2}{2}+\frac{(\eta-1)^3}{3}+\cdots+\frac{(\eta-1)^N}{N}+\cdots \tag{A.3}$$

Combining Eqs. (A.1)–(A.3), (35), (36), (40) and (41) with two-term Taylor series yields

$$d_{m0}=1$$

$$d_{m1}=0$$

$$d_{m2}=\frac{(M+1)}{8\kappa^2}\lambda_m$$

$$d_{m3}=0$$

$$\vdots$$

$$d_{mn}=\frac{(M+1)}{2\kappa^2[n(n-1)+n]}\lambda_m\left(d_{mn-2}-\frac{d_{mn-4}}{\kappa^2}\right) \tag{A.4}$$

$$e_{m0}=1$$

$$e_{m1}=0$$

$$e_{m2}=-\frac{1}{8}\frac{M}{W_1(1-\kappa^2)}\lambda_m\left(1-\frac{3W_2}{2}\right)$$

$$e_{m3}=-\frac{1}{9}\frac{M}{W_1(1-\kappa^2)}\lambda_m W_2$$

$$\vdots$$

$$e_{mn}=\frac{-M\cdot\lambda_m}{2W_1(1-\kappa^2)[n(n-1)+n-1]}\times\left[\left(1-\frac{3W_2}{2}\right)e_{mn-2}+2W_2e_{mn-3}-\left(1+\frac{W_2}{2}\right)e_{mn-4}\right] \tag{A.5}$$

for flow pattern A, and

$$
\begin{aligned}
d_{m0} &= 1 \\
d_{m1} &= 0 \\
d_{m2} &= -\frac{M}{8\kappa^2}\lambda_m \\
d_{m3} &= 0 \\
&\vdots \\
d_{mn} &= -\frac{M}{2\kappa^2[n(n-1)+n]}\lambda_m\left(d_{mn-2}-\frac{d_{mn-4}}{\kappa^2}\right) \qquad \text{(A.6)} \\
e_{m0} &= 1 \\
e_{m1} &= 0 \\
e_{m2} &= \frac{1}{8}\frac{(M+1)}{W_1(1-\kappa^2)}\lambda_m\left(1-\frac{3W_2}{2}\right) \\
e_{m3} &= \frac{1}{9}\frac{(M+1)}{W_1(1-\kappa^2)}\lambda_m W_2 \\
&\vdots \\
e_{mn} &= \frac{(M+1)\lambda_m}{2W_1(1-\kappa^2)[n(n-1)+n-1]} \\
&\quad\times\left[\left(1-\frac{3W_2}{2}\right)e_{mn-2}+2W_2e_{mn-3}-\left(1+\frac{W_2}{2}\right)e_{mn-4}\right] \qquad \text{(A.7)}
\end{aligned}
$$

for flow pattern B.

References

[1] R.K. Shah, A.L. London, Laminar Flow Forced Convection in Ducts, Academic Press, New York, 1978, pp. 196–207.

[2] V-D. Dang, M. Steinberg, Convective diffusion with homogeneous and heterogeneous reaction in a tube, J. Phys. Chem. 84 (1980) 214–219.

[3] T.L. Perelman, On conjugated problems of heat transfer, Int. J. Heat Mass Transfer 3 (1961) 293–303.

[4] D. Murkerjee, E.J. Davis, Direct-contact heat transfer immiscible fluid layers in laminar flow, AIChE J. 18 (1972) 94–101.

[5] S.S. Kim, D.O. Cooney, Improved theory for hollow-fiber enzyme reactor, Chem. Eng. Sci. 31 (1976) 289–294.

[6] E.J. Davis, S. Venkatesh, The solution of conjugated multiphase heat and mass transfer problems, Chem. Eng. Sci. 34 (1979) 775–787.

[7] E. Papoutsakis, D. Ramkrishna, Conjugated Graetz problems. I: General formalism and a class of solid–fluid problems, Chem. Eng. Sci. 36 (1981) 1381–1390.

[8] E. Papoutsakis, D. Ramkrishna, Conjugated Graetz problems. II: Fluid–fluid problems, Chem. Eng. Sci. 36 (1981) 1393–1399.

[9] X. Yin, H.H. Bau, The conjugated Graetz problem with axial conduction, Trans. ASME 118 (1996) 482–485.

[10] R.J. Nunge, W.N. Gill, An analytical study of laminar counterflow double-pipe heat exchangers, AIChE J. 12 (1966) 279–289.

[11] H.M. Yeh, S.W. Tsai, C.L. Chiang, Recycle effects on heat and mass transfer through a parallel-plate channel, AIChE J. 33 (1987) 1743–1746.

[12] C.D. Ho, Y.C. Tsai, J.W. Tu, Heat transfer flow in a parallel-plate channel by inserting in parallel impermeable sheets for multi-pass coolers or heaters, Int. J. Heat Mass Transfer 47 (2004) 459–476.

[13] C.D. Ho, H.M. Yeh, S.C. Chiang, A study of mass transfer efficiency in a parallel-plate channel with external refluxes, Chem. Eng. J. 85 (2002) 207–214.

[14] C.D. Ho, H.M. Yeh, J.J. Guo, An analytical study on the enrichment of heavy water in the continuous thermal diffusion column with external refluxes, Sep. Sci. Technol. 37 (2002) 3129–3153.

[15] A. Fadavi, Y. Chisti, Gas–liquid mass transfer in a novel forced circulation loop reactor, Chem. Eng. J. 112 (2005) 73–80.

[16] R. Marquart, Circulation of high-viscosity Newtonian and non-Newtonian liquids in jet loop reactor, Int. Chem. Eng. 20 (1981) 399–407.

[17] M.H. Siegel, J.C. Merchuk, K. Schugerl, Air-lift reactor analysis: interrelationships between riser, downcomer, and gas–liquid separator behavior, including gas recirculation effects, AIChE J. 32 (1986) 1585–1596.

[18] M. Atenas, M. Clark, V. Lazarova, Holdup and liquid circulation velocity in a rectangular air-lift bioreactor, Ind. Eng. Chem. Res. 38 (1999) 944–949.

[19] A.E. Sáez, F.F. Pironti, V.R. Medina, R. Calvo, Effect of draft tube position on the hydrodynamics of a draft tube slurry bubble column, Chem. Eng. J. Biochem. Eng. J. 60 (1995) 155–160.

[20] K.I. Kikuchi, H. Takahashi, Y. Takeda, F. Sugawara, Hydrodynamic behavior of single particles in a draft-tube bubble column, Can. J. Chem. Eng. 77 (1999) 573–578.

[21] C.D. Ho, H.M. Yeh, W.Y. Yang, Improvement in performance on laminar counterflow concentric circular heat exchangers with external refluxes, Int. J. Heat Mass Transfer 45 (2002) 3559–3569.